Temperature and Snowfall in Western Queen Maud Land Increasing Faster Than Climate Model Projections

B. Medley[1] (iD), J. R. McConnell[2], T. A. Neumann[1], C. H. Reijmer[3], N. Chellman[2], M. Sigl[4] (iD), and S. Kipfstuhl[5] (iD)

[1]Cryospheric Sciences Laboratory, NASA Goddard Space Flight Center, Greenbelt, MD, USA, [2]Desert Research Institute, Nevada System of Higher Education, Reno, NV, USA, [3]Institute for Marine and Atmospheric Research Utrecht, Utrecht University, Utrecht, Netherlands, [4]Laboratory of Environmental Chemistry, Paul Scherrer Institute, Villigen, Switzerland, [5]Alfred Wegener Institute, Helmholtz Centre for Polar and Marine Research, Bremerhaven, Germany

Abstract East Antarctic Ice Sheet (EAIS) mass balance is largely driven by snowfall. Recently, increased snowfall in Queen Maud Land led to years of EAIS mass gain. It is difficult to determine whether these years of enhanced snowfall are anomalous or part of a longer-term trend, reducing our ability to assess the mitigating impact of snowfall on sea level rise. We determine that the recent snowfall increases in western Queen Maud Land (QML) are part of a long-term trend ($+5.2 \pm 3.7\%$ decade^{-1}) and are unprecedented over the past two millennia. Warming between 1998 and 2016 is significant and rapid ($+1.1 \pm 0.7$°C decade^{-1}). Using these observations, we determine that the current accumulation and temperature increases in QML from an ensemble of global climate simulations are too low, which suggests that projections of the QML contribution to sea level rise are potentially overestimated with a reduced mitigating impact of enhanced snowfall in a warming world.

Plain Language Summary Climate model projections suggest that increased snowfall over Antarctica, largely due to atmospheric warming, will partly offset dynamic ice losses by the end of the century. There are very few observations, however, that can be used to differentiate between the varying abilities of the climate models to accurately reproduce Antarctic precipitation and temperature. Here we use a 2,000 year record of snowfall and a 19 year record of air temperature to evaluate whether an ensemble of climate model simulations is able to accurately reproduce the observed change at a site in western Queen Maud Land in East Antarctica, where we find that both snowfall and air temperature are significantly increasing. The rates of increase in both snowfall and temperature within the simulations are too low, which suggests a subdued mitigating impact of enhanced snowfall into the future. Observations, especially ones covering a long time period, are few in number but of critical importance in understanding and interpreting climate model projections over the Antarctic Ice Sheet.

1. Introduction

The West Antarctic Ice Sheet (WAIS) is experiencing rapid warming (Bromwich et al., 2013; Steig et al., 2009) and substantial ice mass loss (McMillan et al., 2014; Shepherd et al., 2012; Zwally et al., 2015) designating it as a region vulnerable to change, especially in comparison to the more massive East Antarctic Ice Sheet (EAIS). Researchers typically consider the high and dry EAIS stable, exhibiting little warming (Steig et al., 2009) and no significant change in snowfall (Monaghan et al., 2006) since 1957. Here we present new observations of snow accumulation and air temperature in western Queen Maud Land (QML) that suggest that this region may be experiencing changes at a pace similar to or potentially more rapid than observations from WAIS.

With an ice volume equivalent to 58 m of sea level (Fretwell et al., 2013), Antarctica is the largest store of freshwater on Earth. There is an overwhelming consensus that WAIS is contributing to sea level rise (SLR), the losses being driven largely by glaciers within the Amundsen Sea Embayment including Thwaites and Pine Island glaciers (McMillan et al., 2014; Rignot et al., 2008; Shepherd et al., 2012; Velicogna et al., 2014; Zwally et al., 2015). An intercomparison exercise (Shepherd et al., 2012) found that the EAIS is relatively stable: the 1992–2011 mean annual mass change was statistically indistinguishable from 0. Anomalous snowfall events toward the end of the period, however, led to years of EAIS mass gain, suggesting that the EAIS
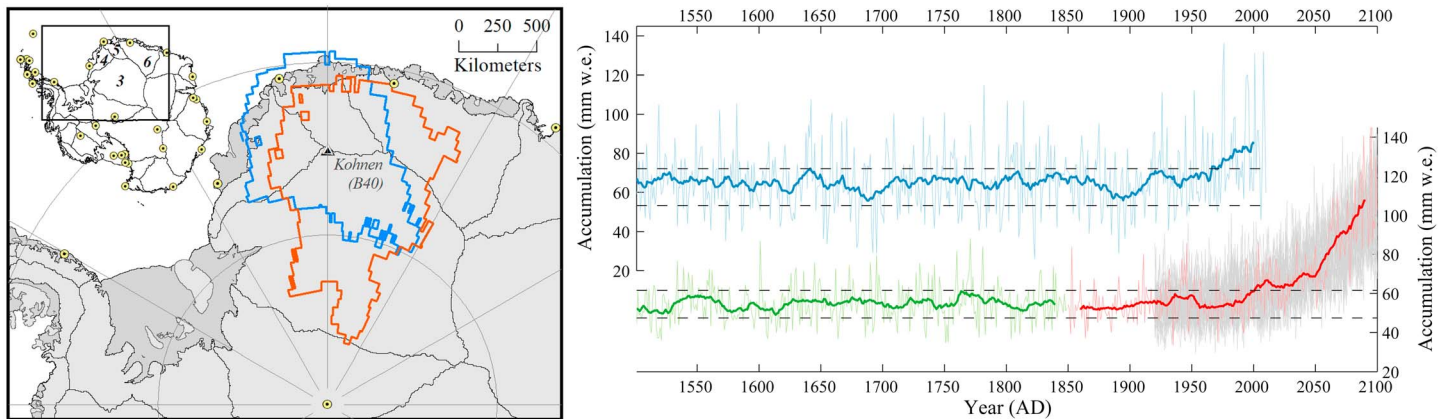
Figure 1. (left) Location of the B40 ice core and AWS (black triangle, left) near Kohnen Station and (right) the truncated time series of annual accumulation from the B40 ice core (top) and CESM (bottom). (Figure 1, left) The region encircled in blue experiences $P - E$ fluctuations that are significantly related (99% confidence interval) to the variations at B40 in all three reanalyses. This produces a minimum bounding geometry of the regions of significance from MERRA-2, CFSR, and ERA-Interim. The red line is the same except for 2 m air temperature. Inset map shows locations of the READER sites, and the numbered basins within have substantial areas relatable to Kohnen climate. The box in the inset shows the bounding area of the main map. MERRA-2 has a grid size of 0.5° latitude × 0.625° longitude, while the CFSR grid is 0.5° × 0.5° and ERA-Interim is 0.75° × 0.75°. (Figure 1, right) Dashed lines bound the upper and lower 2σ around the preindustrial mean. The green line represents the CESM 1850 control run; thus, the years are artificial on the plot prior to 1850. The red line is ensemble member 1 (1850–2100) with its 20 year running mean in bold red, and the gray lines are ensemble members 2–30 (1920–2100). Beginning in 2006, the RCP8.5 high-emission scenario forces the ensemble simulations.

mass balance is dominated by surface mass fluctuations. Conversely, Zwally et al. (2015) reported mass gain from EAIS that is large enough to outweigh WAIS mass losses, postulating that the former is the result of an ice dynamic imbalance due to increased snow accumulation during the Holocene. These results highlight the importance of current and historical snow accumulation in constraining the uncertainty in EAIS mass balance and assessing its contribution to SLR.

We define snow accumulation as the net mass gain of several surface processes including snowfall, sublimation, and blowing snow. Because the latter is minor at the ice sheet scale (Lenaerts et al., 2012), we approximate Antarctic accumulation by creating three atmospheric reanalysis total precipitation-minus-evaporation ($P - E$) products. The data reveal that the 1980–2016 mean annual accumulation over Antarctic grounded ice (and its peripheral islands) is equivalent to 4.9–6.7 mm of sea level. Because the atmospheric moisture holding capacity will increase in a warming climate, snowfall is expected to grow into the future (Genthon et al., 2009; Krinner et al., 2007; Lenaerts et al., 2016; Ligtenberg et al., 2013). This intensified snowfall could mitigate a portion of the anticipated WAIS dynamic losses (DeConto & Pollard, 2016; Joughin et al., 2014), and we thus recognize that analyzing past, present, and future changes in EAIS snow accumulation is a critical exercise to understand the future mass balance of the Antarctic Ice Sheet (AIS). Here we focus specifically on changes in western QML.

We present a snow accumulation record derived from a shallow ice core (165 m) near Kohnen Station (75.0°S, 0.07°E)—hereinafter called "B40"—that spans 1–2010 CE to understand how recent environmental changes observed in western QML relate to historical values (Figure 1). An automatic weather station (AWS) nearby (75.0°S, 0.01°E) provides additional constraint on recent temperature change. While our data derive from a specific location, atmospheric models indicate that these measurements represent a broader area (Figure 1).

Reanalysis $P - E$ indicates that B40 is representative of Zwally et al. (2012) drainage basins 4 and 5, which respectively correspond to Coats Land and the Jutulstraumen glacier catchment, and the northern sector of basin 3 (the upper Slessor glacier catchment) (see Figure 1 inset). Regression analysis allowed us to evaluate whether change in $P - E$ at B40 translates into change at other locations and was performed using three reanalysis models (see section 2.3). We find that the B40 record is likely representative of change within the region that is significantly related (at the 99% confidence level) to B40 $P - E$ in all three reanalyses (Figure 1, red line). By limiting the region to the sector where significance occurs in all three reanalyses, we reduce the

likelihood of overestimating the regional representativeness of the site. The grounded ice within the region of significance amounts to ~7% of the entire AIS. Thus, changes at B40 are representative of an area that is large enough to receive a substantial portion of AIS-wide snowfall.

Regression analysis of 2 m air temperature reveals that the AWS is representative of a region similar to $P - E$ but with distinct differences. Notably, the AWS temperature record is significantly related to temperatures over the plateau, extending farther south and not over the northern ice shelves and islands. The representative region for 2 m air temperature comprises ~10% of the grounded AIS. Thus, the AWS temperature changes observed at Kohnen are likely most representative of the high plateau region of western QML, which is substantiated by evaluation of 2 m air temperature trends in NASA Modern Era Retrospective Analysis for Research and Applications version 2 (MERRA-2) (supporting information Figures S1–S3).

2. Data and Methods

2.1. Ice Core Analysis and Strain Correction

A broad range of elements and chemical species were measured continuously in the B40 ice core with a well-established ice core analytical system (McConnell et al., 2002). These results were used to identify annual layers in the chemistry records using a multiparameter approach. Volcanic synchronization to the well-dated WAIS Divide ice core on the WD2014 timescale (Sigl et al., 2015) was used to constrain the relative annual layer counting. Confirmation of the accuracy in annual layer counting during recent decades to centuries comes from detailed comparisons of the continuous plutonium (Arienzo et al., 2016) and lead pollution (McConnell et al., 2014) records in the B40 core with other well-dated ice cores from Antarctica.

The density profile necessary for conversion of the annual layer thickness record from firn depth to ice- and water-equivalent depths was determined by fitting a high-order polynomial to the measured mass-to-volume ratio of each core section. Potential bias in the density profile largely resulted from overestimation of the volume, which translates into underestimation of the density and annual net accumulation in the shallower parts of the profile. For B40, we estimated a maximum underestimation of 10% at the surface, declining to 5% at 3.5 m depth (~1997 CE) and <2% at 11 m (~1945 CE) and deeper. While not included, these biases would only enhance the relative difference between modern-day and preindustrial values; thus, the recent accumulation increase is likely a lower bound on the actual change.

When developing the B40 accumulation record, the measured depth-dependent density was used to convert each annual layer thickness into an ice-equivalent thickness. We then account for the vertical strain experienced by each annual layer due to ice flow. If ignored, our record would increasingly underestimate annual accumulation for progressively older ice. The core is shallow (165 m) relative to the ice thickness (2750 m), so most of the vertical strain is from densification, and correction for ice flow is done using a simple flow model (Dansgaard & Johnsen, 1969). Assuming divide flow (B40 is <2H from the divide, where H is the ice thickness), we apply a strain correction to the B40 ice-equivalent accumulation. The accumulated strain at the bottom of B40 is roughly 9%. Low surface velocity ($< 5 \text{ m yr}^{-1}$) indicates that corruption of the record by ice flow around topography is negligible and that the record should be dominated by a climatic signal. After correction, we convert the ice-equivalent accumulation into water-equivalent (w.e.).

2.2. Automatic Weather Station Near-Surface Temperature

The weather station near Kohnen was installed in December 1997 and has been operational since. The station measures air temperature, relative humidity, wind speed and direction, instrument height, air pressure, incoming and reflected short wave radiation, incoming and outgoing long wave radiation, and snow temperature. Sensor specifications are published in van den Broeke et al. (2004). The station is powered by lithium batteries and samples every 6 min after which 2-hourly (1997–2001) or 1-hourly (2001 to present) means are calculated, stored locally, and transmitted using Argos transmitters. The sensors are not ventilated for reasons of energy efficiency, which may affect the accuracy of the air temperature sensor among others. The magnitude of the resulting error depends on the amount of incoming and reflected solar radiation, the wind speed, and the type of radiation shield used (Van As et al., 2005). Due to the low temperatures encountered at the site, some of the sensors operated outside their operational specifications. For this reason, the station was equipped with different temperature sensor in 2008.

2.3. Global Atmospheric Models

We created $P - E$ products from three global reanalysis products, specifically the European Centre for Medium-Range Weather Forecasts "Interim" (ERA-Interim) (Dee et al., 2011), the NASA Modern Era Retrospective Analysis for Research and Applications version 2 (MERRA-2) (Gelaro et al., 2017), and the National Centers for Environmental Prediction Climate Forecast System Reanalysis (CFSR) (Saha et al., 2010). To facilitate comparison between products, we use their common time interval, 1980–2016. To create mean annual snow accumulation, the monthly $P - E$ products are accumulated by year and then averaged over the 1980–2016 interval. The gridded products, which have different grid geometries, were reprojected onto a common 5 km equal-area polar grid. The grounded ice sheet area is defined by the area enclosed by the 27 NASA drainage system boundaries (Zwally et al., 2012).

To facilitate assessment of climate change in the presence of internal climate variability, the Community Earth System Model (CESM) community created the Large Ensemble project (Kay et al., 2015), a 30-member ensemble of simulations using CESM1 (Hurrell et al., 2013). To spin up the climate system and initialize these simulations, a 2,200 year simulation of the preindustrial climate was generated, which we use here (years 401–2200) to determine internal climate variability without human-induced climate change. The 30 ensemble members cover most of the 20th and the entire 21st century (1920–2100), one of which covers the entire period since the preindustrial (1850–2100). Beyond 2006, the representative concentration pathway 8.5 (RCP8.5) forcing (van Vuuren et al., 2011) is used. For this work, we used $P - E$ and 2 m air temperature outputs, which are available at ~1° horizontal resolution, and all distributions presented include results from all 30 ensemble members. All results from CESM-LE are based on the time series belonging to the grid cell in which Kohnen is located.

We use CESM-LE because the multimember ensemble allows for statistical determination of the internal variability of the climate system. Other climate models participating in the Coupled Model Intercomparison Project Phase 5 (CMIP5) do not provide as robust an ensemble, so similar analyses are not performed. Palerme et al. (2017) found that only one third of the CMIP5 models generate present-day snowfall rates similar to remotely sensed observations, suggesting that projections from this subset are more reliable. The large ensemble simulations were performed using the CESM1-CAM5 model, which was one of the few that reproduced present-day observations and Antarctic surface mass balance better than several other CMIP5 models (Agosta et al., 2015). Palerme et al. (2017) determined that these reliable models exhibited stronger temperature and precipitation increases over the 21st century than the entire CMIP5 ensemble. While we do not evaluate other models, results from Palerme et al. (2017) suggest that the increases in temperature and precipitation from CESM-LE are likely on the upper end of the CMIP5 models.

2.4. Evaluating Accumulation Sensitivity to Temperature

Using the $P - E$ outputs from the global reanalyses and CESM-LE in combination with their 2 m air temperature, we calculate the accumulation sensitivity to temperature. We determine the slope of a linear fit between the annually resolved model outputs by minimizing the perpendicular distance from each variable pair to the regression model (supporting information Figure S4). This technique is more appropriate than traditional linear regression, which minimizes the dependent variable's distance to the linear model. Under traditional regression, inverting the slope does not produce the same slope as swapping dependent and independent variables, which does not suitably capture the relationship between the two variables. Because there are changes in temperature and accumulation that are not directly related to one another, it is important to minimize the perpendicular distance as it incorporates the variability of both the independent and dependent variables. The presented uncertainties in the accumulation sensitivity represent the 95% confidence bounds to the regression model fit.

2.5. Trend Calculation and Uncertainty

We perform traditional least squares regression to determine the trend in both the ice core and atmospheric model accumulation and temperature time series over the specified time intervals. Calculation of the trend uncertainty accounts for the reduction in independent samples due to autocorrelation within the record (Santer et al., 2000).

Errors in the density profile might also generate false trends in the B40 time series, especially near the surface where density is the lowest. Using a Monte Carlo method, we approximate the uncertainty in our B40 trend

analysis resulting from random deviations in the density profile based on the polynomial fit to the measured density profile and its 2σ bounds (see supporting information). Not surprisingly, trend uncertainty due to density perturbations increases for more recent trends. On average, uncertainty in the preindustrial trends is ±2.4 mm w.e. per century or about one third of the measured standard deviation in B40 preindustrial trends (7.0 mm w.e. per century) and likely does not impact the distribution. For modern trends (1920–1936), the average trend uncertainty is ±3.6 mm w.e. per century, which comprises just over 10% of the observed modern trend ($m_{75} = 29.7$ mm w.e. per century). While uncertainties in the density could generate a false trend in accumulation, the magnitude of change between the preindustrial and modern trends is large enough to outweigh the potential misrepresentation of change. Because B40 is in a divide flow regime where strain rate increases linearly with depth, both the preindustrial and modern trends are on average ~0.3 mm w.e. per century less than in the uncorrected time series. Therefore, relative change between the two periods is not impacted and uncertainty from errors in firn density dominates.

3. Results

3.1. Observed Increase in Snow Accumulation

The B40 annual record and 20 year running mean are displayed in Figure 1 and truncated to begin in 1500. The entire record is in supporting information Figure S8. The preindustrial statistics are based on the period from 1 to 1850 CE, and changing our definition of the preindustrial (Hawkins et al., 2017) does not significantly impact the results.

We first evaluate recent 20 year accumulation means (A_{20}) relative to the B40 preindustrial population (Figure 2a) to assess whether the current climate conditions are outside of the bounds of natural variability. Modern-day A_{20} have initial years between 1980 and 1991 and provide the basis for comparison with preindustrial values (Figure 2a). Prior to 1850, A_{20} are normally distributed ($\mu = 66.2$, $\sigma = 3.2$ mm w.e.), and comparison with values since 1980 suggests that accumulation is significantly larger than the preindustrial ($>5\sigma$, $p = 1.5e{-}7$). Specifically, A_{20} is on average 16.5 mm w.e. larger, which is 25% higher than the preindustrial mean. The A_{20} since 1972 are larger than all the preindustrial values and are increasing in time; therefore, current accumulation rates at B40 are neither representative of the long-term mean nor are within the expected natural variability.

Similarly, recent 75 year trends (m_{75}) are significantly larger than the majority from the preindustrial period (Figure 2b). Modern-day m_{75} begin in 1920 to overlap with the initial year in the CESM-LE members 2–30. All but one of m_{75} since 1920 are larger than the preindustrial trends ($\mu = 0.19$, $\sigma = 7.0$ mm w.e. century^{-1}) and lie beyond $+4\sigma$ ($p = 8.5e{-}6$) of the preindustrial distribution. Modern (since 1920) trends indicate that B40 snow accumulation is increasing 29.7 mm w.e. century^{-1} on average, which is equivalent to $+45\%$ of the preindustrial mean every 100 years. Bolstering our confidence in a regional increase in snow accumulation, we find that existing QML records substantiate the modern increases observed in the B40 record (see supporting information).

3.2. Evaluation of Model Precipitation Minus Evaporation

Analysis of CESM-LE $P - E$ (Figure 1) reveals that the preindustrial distributions of A_{20} and m_{75} are markedly similar to those observed in B40 (Figure 2c,d). In both instances, the standard deviation of the CESM-LE distribution is smaller than B40, which is expected considering that the CESM-LE control run is an evaluator of the internal variability of the climate system, whereas B40 has additional structure due to actual climate changes and glaciological noise. These results indicate that the CESM-LE preindustrial simulation suitably represents natural climate variability.

We find that A_{20} are expected to grow in the future, and the widening distributions with time suggest more variability in the simulations (Figure 2c). The result is similar when evaluating present and future m_{75}: the trend magnitude and variability will increase moving toward the end of the 21st century (Figure 2d). Neither of these findings are notable; AIS snow accumulation is expected to increase under a warming climate (Genthon et al., 2009; Krinner et al., 2007; Lenaerts et al., 2016; Ligtenberg et al., 2013). Observed changes from the B40, however, are largely outpacing those from CESM-LE, even under warmer temperatures predicted by the high-emission RCP8.5 scenario. Remarkably, the changes currently observed at B40 occur several decades later in the CESM-LE output. Thus, current and potentially future accumulation
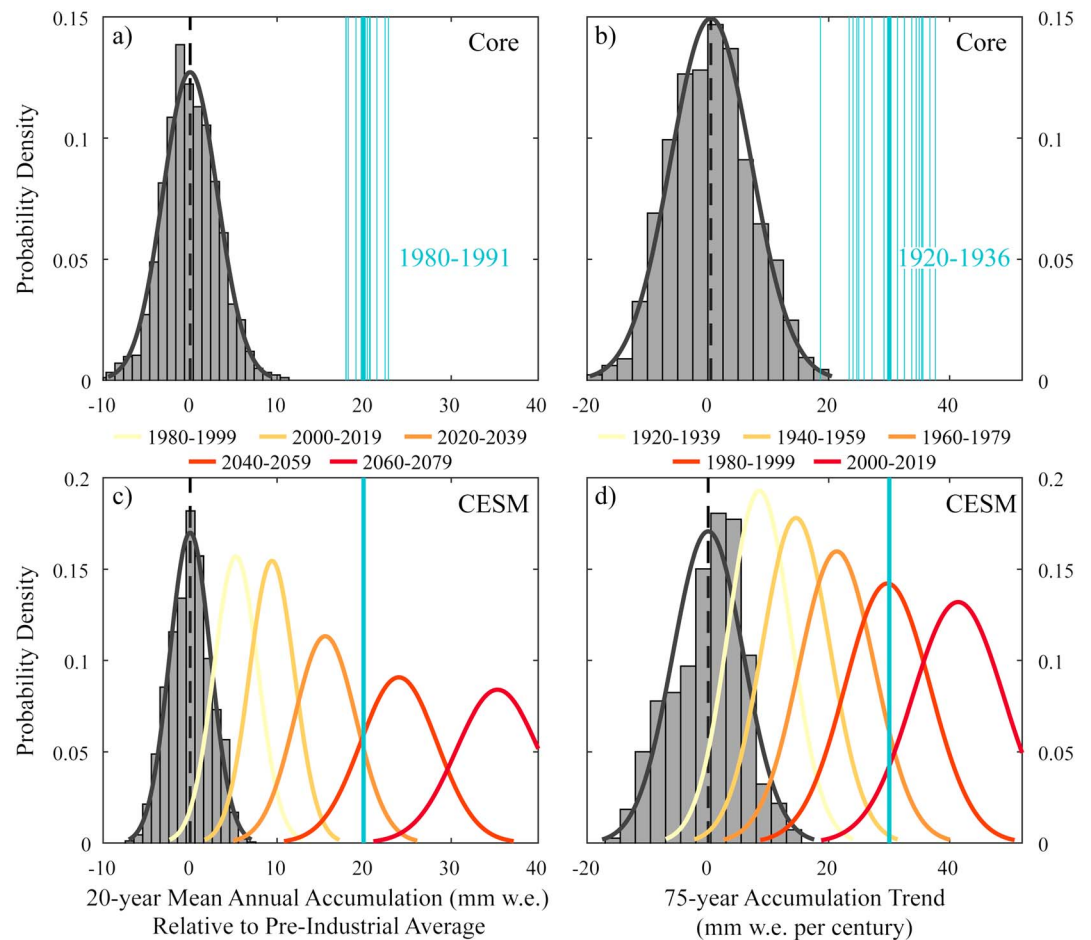
Figure 2. (a, b) Core and (c, d) model distributions of 20 year mean annual accumulation (Figures 2a and 2c) and 75 year trends (Figures 2b and 2d) for preindustrial and modern-day values. Gray histograms represent preindustrial values for both the core and model data. A CESM 2,000 year run with constant forcings representative of the climate system in 1850 provides the preindustrial values, and it provides a measure of the internal variability of the system. For the core, preindustrial values include all data values prior to 1850. Pale blue lines represent individual years from the modern day (Figure 2a: 1980–1991; Figure 2b: 1920–1936), and the bold blue line is the average of these values. The model plots (Figures 2c and 2d) also include distributions from their 30-member ensemble over 20 year time intervals.

changes near Kohnen Station are likely more rapid than found in CESM-LE, which has important implications for future projections of western QML mass balance. If the rates of accumulation increase are larger than the modeled values, the impact of additional snowfall on reducing the AIS contribution to SLR will be diminished in projections.

3.3. Snow Accumulation Sensitivity to Temperature

Several studies (Frieler et al., 2015; Monaghan & Bromwich, 2008; Monaghan et al., 2008; Smith et al., 1998; van Lipzig et al., 2002) have investigated the direct relationship between snow accumulation and temperature: warmer temperatures are associated with more snow accumulation. By quantifying this relationship, the B40 change in snow accumulation can be translated into temperature change. The relationship between temperature and accumulation varies slightly depending on the atmospheric model, so a range of sensitivities are provided (supporting information Figure S4). We use the 1980–2016 $P - E$ and 2 m temperature products from CESM-LE member 1, ERA-Interim, and MERRA-2 because the CFSR output shows spurious jumps in temperature. ERA-Interim and MERRA-2 have remarkably similar sensitivities of 19.4 ± 9.9 and 18.7 ± 8.6 mm w.e. °C^{-1}, whereas CESM-LE suggests a weaker sensitivity of 16.8 ± 9.3 mm w.e. °C^{-1}. These values indicate
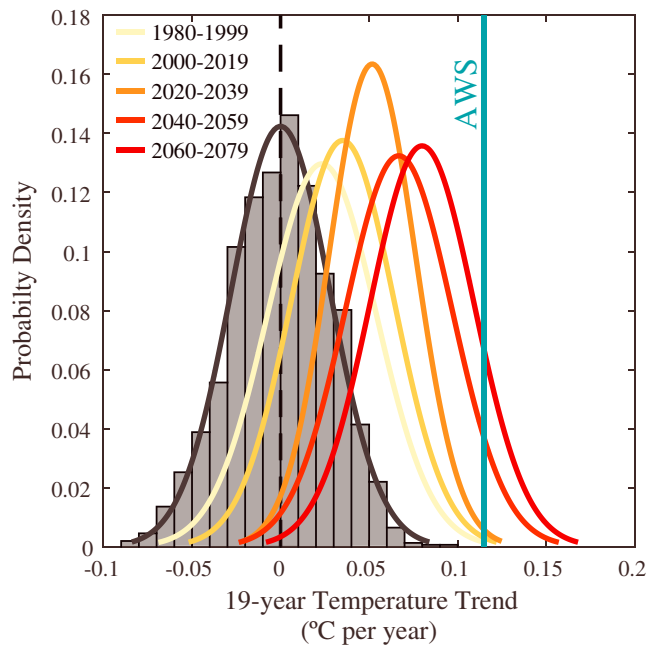
Figure 3. Distribution of 19 year temperature trends from the CESM 1850 control run (gray histogram) as well as current and future trends beginning in 1980 from a 30-member ensemble. The blue line is the current 1998–2016 observed annual temperature trend from an AWS at Kohnen.

that recent (1980–2010) temperatures are on average ~0.9–1.0°C warmer than the preindustrial average, based on the accumulation increase of 16.5 mm w.e. observed in the B40 record. Thus, Kohnen Station and potentially much of western QML are warmer and wetter presently than most of the prior two millennia.

3.4. Observed Increase in Air Temperature

Unlike snow accumulation which has a recoverable signal, no long-term historical records of air temperature exist at this remote site. AWS measurements covering a 19 year interval between 1998 and 2016 reveal that Kohnen Station is warming annually at a rate of 1.15 ± 0.71°C decade^{-1} with significant warming during autumn (March-April-May: 2.53 ± 1.93°C decade^{-1}) and spring (September-October-November: 1.44 ± 0.89°C decade^{-1}; supporting information Figure S1). Insignificant increases and decreases in temperature were found in summer (December-January-February: 1.17 ± 1.28°C decade^{-1}) and winter (June-July-August: −0.30 ± 1.53°C decade^{-1}), respectively. The annual warming is larger than the 38 complete contemporaneous records within the REference Antarctic Data for Environmental Research (READER) database (Turner et al., 2004; supporting information Figure S12), out of which only one nearby site underwent significant warming: Amundsen-Scott South Pole Station (0.87 ± 0.70°C decade^{-1}; Figure 1). Our results suggest that Kohnen likely experienced more rapid warming than several coastal and inland sites around the AIS and that much of the western QML high plateau potentially warmed as well (Figure 1, red line).

3.5. Evaluation of Model 2 m Temperature

Because the CESM-LE preindustrial $P - E$ adequately represented the internal variability at Kohnen Station, we assume the same for preindustrial 2 m temperature. Using a similar approach as done with snow accumulation trends, we compare the observed AWS temperature trend to 19 year trends from the CESM-LE, both baseline preindustrial and the 20th and 21st centuries (Figure 3). As expected, the preindustrial distribution is symmetric around 0, which begins to shift toward more positive values moving into the future. Interestingly, the AWS trend of 1.1°C decade^{-1} is an unlikely member of the CESM-LE modern (1980–1999) trends and is more consistent with trends after 2040. This comparison suggests that CESM-LE is potentially underestimating current temperature change and that changes expected decades into the future are occurring presently, which substantiates the results from the comparison with B40. The AWS and B40 records independently point toward earlier onset of rapid change than the CESM-LE simulations, and the corroborating evaluations of CESM-LE accumulation and temperature adds confidence to our interpretation (i.e., diminished accumulation change should be accompanied by diminished temperature change).

4. Conclusions

We find that western QML is undergoing rapid climate change that is likely not sufficiently represented in CESM-LE future projections. We conclude the following:

1. The recent climate at Kohnen Station is not representative of the long-term mean and is significantly wetter than the nearly 2,000 years prior (1–1850 CE). Recent snow accumulation is 25% larger, and annual air temperatures are on average 0.9–1.0°C warmer than the preindustrial. We conclude that "anomalous" snowfall gains in QML over recent years, responsible for years of mass gain over EAIS (Shepherd et al., 2012), are likely part of a longer-term trend. Ice core evidence of increased snow accumulation in eastern QML (Philippe et al., 2016) suggests that the pattern might be larger in scale, but a more detailed comparison is necessary to relate the two records. If snow accumulation continues to increase at modern rates (+45% per century), QML snowfall could mitigate sea level contributions from ice loss in WAIS and the Antarctic Peninsula.

2. Small biases in the rates of present and future accumulation change yield large uncertainties in AIS mass balance. The $P - E$ trends in CESM-LE simulations are lower than observed accumulation trends, which suggests that future accumulation in western QML is underestimated. Therefore, the mitigating impact of higher snowfall rates is likely not fully resolved. Between 1990–1999 and 2090–2099, snow accumulation over the grounded AIS increases ~1.5 mm sea level equivalent yr^{-1} in CESM-LE, a value approximately half of the current rate of global mean SLR since 1993 (Beckley et al., 2010) and more than 7 times the current rate of mass loss from the entire AIS (Shepherd et al., 2012). There is a clear need for improved evaluation of global atmospheric model performance in Antarctica since accumulation partly controls the ice sheet's contribution to SLR, which is only possible with more long-term records of accumulation and temperature. Records collected widely across the AIS, covering a substantial portion of the preindustrial through present day, are lacking, yet needed.

References

Agosta, C., Fettweis, X., & Datta, R. (2015). Evaluation of the CMIP5 models in the aim of regional modelling of the Antarctic surface mass balance. *The Cryosphere*, 9(6), 2311–2321. https://doi.org/10.5194/tc-9-2311-2015

Arienzo, M. M., McConnell, J. R., Chellman, N., Criscitiello, A. S., Curran, M., Fritzsche, D., … Opel, T. (2016). A method for continuous ^{239}Pu determinations in Arctic and Antarctic ice cores. *Environmental Science & Technology*, 50(13), 7066–7073. https://doi.org/10.1021/acs.est.6b01108

Beckley, B., Zelensky, N., Holmes, S., Lemoine, F., Ray, R., Mitchum, G., … Brown, S. (2010). Assessment of the Jason-2 extension to the TOPEX/Poseidon, Jason-1 sea-surface height time series for global mean sea level monitoring. *Marine Geodesy*, 33, 447–471. https://doi.org/10.1080/01490419.2010.491029

Bromwich, D. H., Nicolas, J. P., Monaghan, A. J., Lazzara, M. A., Keller, L. M., Weidner, G. A., & Wilson, A. B. (2013). Central west Antarctica among the most rapidly warming regions on earth. *Nature Geoscience*, 6(2), 139–145. https://doi.org/10.1038/ngeo1671

Dansgaard, W., & Johnsen, S. (1969). A flow model and a time scale for the ice core from Camp Century, Greenland. *Journal of Glaciology*, 8(53), 215–223. https://doi.org/10.1017/S0022143000031208

DeConto, R. M., & Pollard, D. (2016). Contribution of Antarctica to past and future sea-level rise. *Nature*, 531(7596), 591–597. https://doi.org/10.1038/nature17145

Dee, D. P., Uppala, S. M., Simmons, A. J., Berrisford, P., Poli, P., Kobayashi, S., … Vitart, F. (2011). The ERA-Interim reanalysis: Configuration and performance of the data assimilation system. *Quarterly Journal of the Royal Meteorological Society*, 137(656), 553–597. https://doi.org/10.1002/qj.828

Fretwell, P., Pritchard, H. D., Vaughan, D. G., Bamber, J. L., Barrand, N. E., Bell, R., … Zirizzotti, A. (2013). Bedmap2: Improved ice bed, surface and thickness datasets for Antarctica. *The Cryosphere*, 7(1), 375–393. https://doi.org/10.5194/tc-7-375-2013

Frieler, K., Clark, P. U., He, F., Buizert, C., Reese, R., Ligtenberg, S. R., … Levermann, A. (2015). Consistent evidence of increasing Antarctic accumulation with warming. *Nature Climate Change*, 5, 348–352.

Gelaro, R., McCarty, W., Suárez, M. J., Todling, R., Molod, A., Takacs, L., … Zhao, B. (2017). The Modern-Era Retrospective Analysis for Research and Applications, version 2 (MERRA-2). *Journal of Climate*, 30(14), 5419–5454. https://doi.org/10.1175/JCLI-D-16-0758.1

Genthon, C., Krinner, G., & Castebrunet, H. (2009). Antarctic precipitation and climate-change predictions: Horizontal resolution and margin vs plateau issues. *Annals of Glaciology*, 50(50), 55–60. https://doi.org/10.3189/172756409787769681

Hawkins, E., Ortega, P., Suckling, E., Schurer, A., Hegerl, G., Jones, P., … Mignot, J. (2017). Estimating changes in global temperature since the pre-industrial period. *Bulletin of the American Meteorological Society*. https://doi.org/10.1175/BAMS-D-16-0007.1

Hurrell, J. W., Holland, M. M., Gent, P. R., Ghan, S., Kay, J. E., Kushner, P. J., … Lindsay, K. (2013). The Community Earth System Model: A framework for collaborative research. *Bulletin of the American Meteorological Society*, 94(9), 1339–1360.

Joughin, I., Smith, B. E., & Medley, B. (2014). Marine ice sheet collapse potentially under way for the Thwaites Glacier basin, west Antarctica. *Science*, 344(6185), 735–738. https://doi.org/10.1126/science.1249055

Kay, J., Deser, C., Phillips, A., Mai, A., Hannay, C., Strand, G., … Edwards, J. (2015). The Community Earth System Model (CESM) large ensemble project: A community resource for studying climate change in the presence of internal climate variability. *Bulletin of the American Meteorological Society*, 96(8), 1333–1349.

Krinner, G., Magand, O., Simmonds, I., Genthon, C., & Dufresne, J. (2007). Simulated Antarctic precipitation and surface mass balance at the end of the twentieth and twenty-first centuries. *Climate Dynamics*, 28(2-3), 215–230. https://doi.org/10.1007/s00382-006-0177-x

Lenaerts, J. T. M., van den Broeke, M. R., van de Berg, W. J., van Meijgaard, E., & Kuipers Munneke, P. (2012). A new, high-resolution surface mass balance map of Antarctica (1979–2010) based on regional atmospheric climate modeling. *Geophysical Research Letters*, 39, L04501. https://doi.org/10.1029/2011GL050713

Lenaerts, J. T. M., Vizcaino, M., Fyke, J., van Kampenhout, L., & van den Broeke, M. R. (2016). Present-day and future Antarctic ice sheet climate and surface mass balance in the Community Earth System Model. *Climate Dynamics*, 47, 1367–1381.

Ligtenberg, S. R. M., van de Berg, W. J., van den Broeke, M. R., Rae, J., & van Meijgaard, E. (2013). Future surface mass balance of the Antarctic ice sheet and its influence on sea level change, simulated by a regional atmospheric climate model. *Climate Dynamics*, 41(3-4), 867–884. https://doi.org/10.1007/s00382-013-1749-1

McConnell, J. R., Lamorey, G. W., Lambert, S. W., & Taylor, K. C. (2002). Continuous ice-core chemical analyses using inductively coupled plasma mass spectrometry. *Environmental Science & Technology*, 36(1), 7–11. https://doi.org/10.1021/es011088z

McConnell, J. R., Maselli, O. J., Sigl, M., Vallelonga, P., Neumann, T., Anschütz, H., … Edwards, R. (2014). Antarctic-wide array of high-resolution ice core records reveals pervasive lead pollution began in 1889 and persists today. *Scientific Reports*, 4, 5848.

McMillan, M., Shepherd, A., Sundal, A., Briggs, K., Muir, A., Ridout, A., … Wingham, D. (2014). Increased ice losses from Antarctica detected by CryoSat-2. *Geophysical Research Letters*, 41, 3899–3905. https://doi.org/10.1002/2014GL060111

Monaghan, A. J., & Bromwich, D. H. (2008). Advances in describing recent Antarctic climate variablity. *Bulletin of the American Meteorological Society*, 89(9), 1295–1306. https://doi.org/10.1175/2008BAMS2543.1

Monaghan, A. J., Bromwich, D. H., Fogt, R. L., Wang, S., Mayewski, P. A., Dixon, D. A., … Wen, J. (2006). Insignificant change in Antarctic snowfall since the international geophysical year. *Science*, 313(5788), 827–831. https://doi.org/10.1126/science.1128243

Monaghan, A. J., Bromwich, D. H., & Schneider, D. P. (2008). Twentieth century Antarctic air temperature and snowfall simulations by IPCC climate models. *Geophysical Research Letters*, *35*, L07502. https://doi.org/10.1029/2007GL032630

Palerme, C., Genthon, C., Claud, C., Kay, J. E., Wood, N. B., & L'Ecuyer, T. (2017). Evaluation of current and projected Antarctic precipitation in CMIP5 models. *Climate Dynamics*, *48*(1-2), 225–239. https://doi.org/10.1007/s00382-016-3071-1

Philippe, M., Tison, J. L., Fjøsne, K., Hubbard, B., Kjær, H. A., Lenaerts, J. T., … Pattyn, F. (2016). Ice core evidence for a 20th century increase in surface mass balance in coastal Dronning Maud Land, East Antarctica. *The Cryosphere*, *10*(5), 2501. https://doi.org/10.5194/tc-10-2501-2016

Rignot, E., Bamber, J. L., van den Broeke, M. R., Davis, C., Li, Y., van de Berg, W. J., & van Meijgaard E. (2008). Recent Antarctic ice mass loss from radar interferometry and regional climate modelling. *Nature Geoscience*, *1*(2), 106–110. https://doi.org/10.1038/ngeo102

Saha, S., Moorthi, S., Pan, H., Wu, X., Wang, J., Nadiga, S., … Goldberg, M. (2010). The NCEP climate forecast system reanalysis. *Bulletin of the American Meteorological Society*, *91*(8), 1015–1058. https://doi.org/10.1175/2010BAMS3001.1

Santer, B. D., Wigley, T., Boyle, J., Gaffen, D. J., Hnilo, J., Nychka, D., … Taylor, K. (2000). Statistical significance of trends and trend differences in layer-average atmospheric temperature time series. *Journal of Geophysical Research*, *105*(D6), 7337–7356. https://doi.org/10.1029/1999JD901105

Shepherd, A., Ivins, E. R., A, G., Barletta, V. R., Bentley, M. J., Bettadpur, S., … Zwally, H. J. (2012). A reconciled estimate of ice-sheet mass balance. *Science*, *338*(6111), 1183–1189. https://doi.org/10.1126/science.1228102

Sigl, M., Winstrup, M., McConnell, J., Welten, K., Plunkett, G., Ludlow, F., … Dahl-Jensen, D. (2015). Timing and climate forcing of volcanic eruptions for the past 2,500 years. *Nature*, *523*(7562), 543–549. https://doi.org/10.1038/nature14565

Smith, I., Budd, W., & Reid, P. (1998). Model estimates of Antarctic accumulation rates and their relationship to temperature changes. *Annals of Glaciology*, *27*(1), 246–250. https://doi.org/10.3189/1998AoG27-1-246-250

Steig, E. J., Schneider, D. P., Rutherford, S. D., Mann, M. E., Comiso, J. C., & Shindell, D. T. (2009). Warming of the Antarctic ice-sheet surface since the 1957 international geophysical year. *Nature*, *457*(7228), 459–462. https://doi.org/10.1038/nature07669

Turner, J., Colwell, S. R., Marshall, G. J., Lachlan-Cope, T. A., Carleton, A. M., Jones, P. D., … Iagovkina, S. (2004). The SCAR READER project: Toward a high-quality database of mean Antarctic meteorological observations. *Journal of Climate*, *17*(14), 2890–2898. https://doi.org/10.1175/1520-0442(2004)017%3C2890:TSRPTA%3E2.0.CO;2

Van As, D., Van Den Broeke, M., & Van De Wal, R. (2005). Daily cycle of the surface layer and energy balance on the high Antarctic plateau. *Antarctic Science*, *17*(1), 121.

van den Broeke, M. R., Reijmer, C. H., & van de Wal, R. S. W. (2004). A study of the surface mass balance in Dronning Maud Land, Antarctica, using automatic weather stations. *Journal of Glaciology*, *50*(171), 565–582. https://doi.org/10.3189/172756504781829756

van Lipzig, N. P., van Meijgaard, E., & Oerlemans, J. (2002). Temperature sensitivity of the Antarctic surface mass balance in a regional atmospheric climate model. *Journal of Climate*, *15*(19), 2758–2774. https://doi.org/10.1175/1520-0442(2002)015%3C2758:TSOTAS%3E2.0.CO;2

van Vuuren, D. P., Edmonds, J., Kainuma, M., Riahi, K., Thomson, A., Hibbard, K., … Lamarque, J. (2011). The representative concentration pathways: An overview. *Climatic Change*, *109*(1-2), 5–31. https://doi.org/10.1007/s10584-011-0148-z

Velicogna, I., Sutterley, T., & Van den Broeke, M. (2014). Regional acceleration in ice mass loss from Greenland and Antarctica using GRACE time-variable gravity data. *Geophysical Research Letters*, *41*, 8130–8137. https://doi.org/10.1002/2014GL061052

Zwally, H. J., Giovinetto, M. B., Beckley, M. A., & Saba, J. L. (2012). Antarctic and Greenland Drainage Systems. *GSFC Cryospheric Sciences Laboratory*. Retrieved from https://icesat4.gsfc.nasa.gov/cryo_data/ant_grn_drainage_systems.php

Zwally, H. J., Li, J., Robbins, J. W., Saba, J. L., Yi, D., & Brenner, A. C. (2015). Mass gains of the Antarctic ice sheet exceed losses. *Journal of Glaciology*, *61*(230), 1019–1036. https://doi.org/10.3189/2015JoG15J071